Aluminum Cratering Relations for In-Situ Detection of Micrometeoroid and Orbital Debris Particle Diameters

Michael D. Bjorkman[(1)]

[(1)] Jacobs Technology, 2101 NASA Parkway, Houston TX, USA

ABSTRACT

The authors developed a new empirical aluminum cratering relation based on the current understanding of the cratering process and crater dimension scaling. The authors performed two-dimensional CTH finite difference hydrocode calculations with three projectile materials, two aluminum alloy target materials and impact speeds ranging from 5 to 80 km/s.

The authors compared Humes crater counts from his S0001 experiment on the space and aft sides LDEF with calculations using the new cratering relation and the MEM 3 micrometeoroid environment model. The comparison showed that the results agreed on average with the observed crater counts to within a factor of 32% on the space end and a factor of 80% on the aft end.

1 INTRODUCTION

Researchers have used crater counts from a number of returned aluminum surfaces for quantifying the micrometeoroid and orbital debris environment. For example, the Solar Max thermal control louvers, the LDEF thermal control panels and the ISS Multipurpose Logistics Module MMOD shields. Inferring the size particle that produced the crater from the crater dimensions is dependent on a reliable crater dimension scaling relation.

The author of the cratering relation typically used today developed it for Apollo in 1968 and biased the derivation towards meteoroid impact speeds and not underestimating the crater dimensions. For these reasons, it may not be the best relation to use for inferring the dimensions of micrometeoroid and orbital debris particles from their crater dimensions. In order to address this question the authors developed a new crater dimension scaling relation using a current understanding of the cratering process and compared the results of crater count calculations with the observed LDEF crater counts.

2 CRATER DIMENSIONS SCALING RELATIONS

Equation 1 is the crater depth, P, scaling relation developed at the Johnson Space Center (JSC) for the Apollo program. [1] JSC engineers used it for the Apollo command and service module and lunar module micrometeoroid impact-risk assessments. Equation 1 depends on the meteoroid diameter d, the target Brinell hardness H, the target density ρ, the meteoroid density δ, the impact speed U, the impact angle β measured from the target normal, and the target elastic longitudinal sound speed c.

$$\frac{P}{d} = 5.24\, d^{0.056} H^{-0.25} \left(\frac{\rho}{\delta}\right)^{-0.50} \left(\frac{U \cos\beta}{c}\right)^{0.67} \quad (1)$$

The coefficient has units of $cm^{-0.056}$, but the equation is otherwise dimensionless.

The author of Eq. 1 pointed out the speed exponent was likely too large [1] and that the speed exponent depends on the projectile size exponent [2]. The present authors would add to the above list of limitations the following:

1. The ballistic limit equation is only a power-law when the impact is so intense that the cratering motions approach point source cratering motions.[3]
2. The target sound speed is an early time variable and is not a parameter of the crater scaling when the impact

is so intense that the cratering motions approach point source cratering motions, i.e., the crater scaling relation is a power-law.[4]

3. The crater depth to diameter ratio is 0.58 for aluminium onto aluminium impacts and not 0.5.[5]

The authors shall develop two equations to update Eq. 1: one for low speed impacts where the cratering motions are affected by the early time variables and the second for large speed impacts where the cratering motions approach those from a point source and the early time variables enter the crater dimension scaling as a single parameter[1]. The authors shall chose a form for the equations so that the low speed equation fairs smoothly into the high-speed equation. Furthermore, the authors assume the projectile equation of state (EOS) and constitutive equation do not affect the final crater dimensions and that the target plastic strain rate dependence is negligible.

The form of the low-speed crater depth relation is constrained by a dimensional analysis. The dimensional analysis is specialized to targets with Mie Gruneisen EOS and perfectly plastic constitutive equations. For this case, the crater depth depends on four projectile parameters (d,U,β,δ), four target EOS parameters (ρ the density, c_0 the bulk wave speed, s the slope of the linear shock-speed particle-speed relation and Γ_0 the Gruneisen gamma) and two target constitutive equation parameters (Y the perfectly plastic strength and ν the Poisson ratio). By the Buckingham pi-theorem, the crater depth and diameter relations are functions of eight dimensionless groups of parameters. [6] Equations 2 and 3 are one choice of dimensionless parameter groupings

$$\frac{P}{d} = f\left(\frac{\rho}{\delta}, \beta, \frac{U}{\sqrt{Y/\varrho}}, \frac{Y}{\varrho c_0^2}, s, \Gamma_0, \nu\right) \tag{2}$$

$$\frac{P}{D} = g\left(\frac{\rho}{\delta}, \beta, \frac{U}{\sqrt{Y/\varrho}}, \frac{Y}{\varrho c_0^2}, s, \Gamma_0, \nu\right) \tag{3}$$

The form of the high-speed crater depth relation and the depth to diameter ratio is

$$\frac{P_{cp}}{d} = K\left(\frac{U\cos\beta}{\sqrt{Y/\varrho}}\right)^{\mu}\left(\frac{\delta}{\varrho}\right)^{\nu} \tag{4}$$

$$\frac{P_{cp}}{D_{cp}} = \text{Const} \tag{5}$$

which follows from a coupling parameter analysis. [4] The coefficient K is independent of the EOS, but the coupling-parameter speed exponent μ is dependent on the EOS. However, Dienes [3] has shown for an ideal gas and uniaxial strain impact that μ is weakly dependent on the EOS. Furthermore, fifty years of impact testing and hydrocode calculations has confirmed that μ is weakly dependent on the EOS for cratering and that $\mu = 0.55$ is a good value for metals. Porous materials are the exception though. Porosities from 30% to 55% in geologic materials reduced μ to values ranging from 0.35 to 0.40. [7]

The authors used the hydrocode CTH [8] to determine the functions f and g in Eqs. 2 and 3 and the coefficient K in Eq. 4.

The first set of calculations determined the coefficient K in Eq. 4. (Housen and Holsapple [8] report that the other empirically derived parameters of Eq. 4 are μ=0.55 and ν=0.40.) The calculations simulated an aluminum sphere striking an aluminum target at 7 km/s. The target used a Mie Gruneisen EOS and a perfectly plastic constitutive equation. The hydrocode study used fixed projectile diameter of 1.23-cm and impact speed of 7-km/s, but varied target strength. The target used a perfectly plastic constitutive equation so that there was no target strain hardening to alter the strength applicable to the scaling. Thus for the first set of calculations Eq. 4 reduces to $P_{cp} = K\, Y^{\mu/2}$. Figure 1 is a plot of the results of the calculations. The black line is a fit with K=0.4174, the desired result.

[1] Called the coupling parameter by Holsapple.

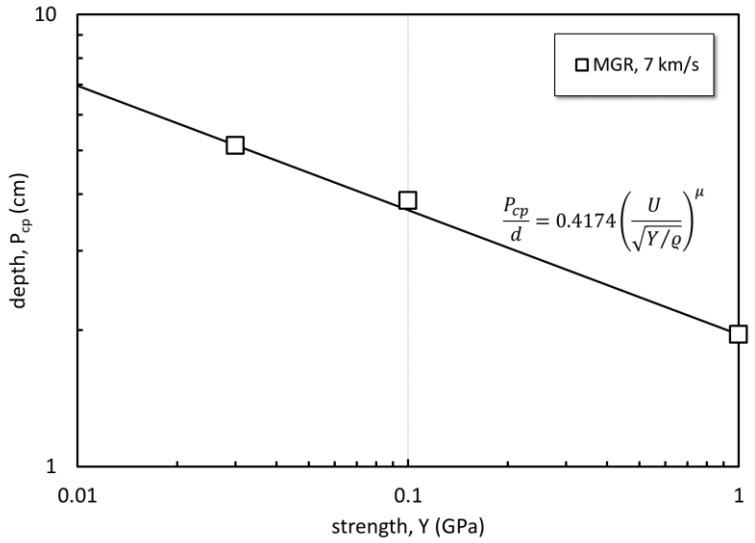

Fig. 1. First hydrocode study results used to determine K in Eq. 4.

The authors use the value of 0.58 for the Eq. 5 constant crater depth to diameter ratio measured by Hörz and coworkers [5] and mentioned above.

The second set of calculations determined the functions f and g in Eqs. 2 and 3. The authors simplified the development of the equations by specializing the equations to 6061-T6. If one specializes Eq. 2 to one target material, then all of the pi-groups composed solely of target parameters are no longer parameters of the crater depth and the last four dimensionless groups of parameters drop out of Eq. 2. Furthermore, the authors assume the normal component of the impact velocity accounts for the impact angle dependence in Eq. 2. Thus, Eq. 2 reduces to

$$\frac{P}{d} = f\left(\frac{\rho}{\delta}, \frac{U\cos\beta}{\sqrt{Y/\varrho}}\right) \tag{6}$$

The CTH calculations simulated the impacts of aluminum and steel spheres onto 6061-T6 aluminum targets. The targets were sufficiently thick that the rear surface reflection did not reach the crater before the simulation stopped. The authors used the SESAME tabular EOS 3700 [9] for aluminum projectiles and the 6061-T6 targets. They used the SESAME tabular EOS 2150 [10] for 304 steel projectiles. They used the Steinberg-Guinan-Lund [11] constitutive equation for the 6061-T6 targets.

Figure 2 shows the results of the CTH crater depth calculations expressed as a normalized difference from the large speed depth, P_{cp}. The square on point symbols plot the CTH crater depths for 304 stainless steel spheres striking 6061-T6 targets. These calculations show that the steel projectiles do not result in the large speed power-law scaling except for speeds larger than those characteristic of meteoroids striking spacecraft in Earth orbit. The circle symbols plot the CTH crater depths for 1100-0 commercially pure aluminum spheres striking 6061-T6 targets. The aluminum projectile crater depths approach the large speed power-law scaling limit for 5-km/s impact speeds and larger.

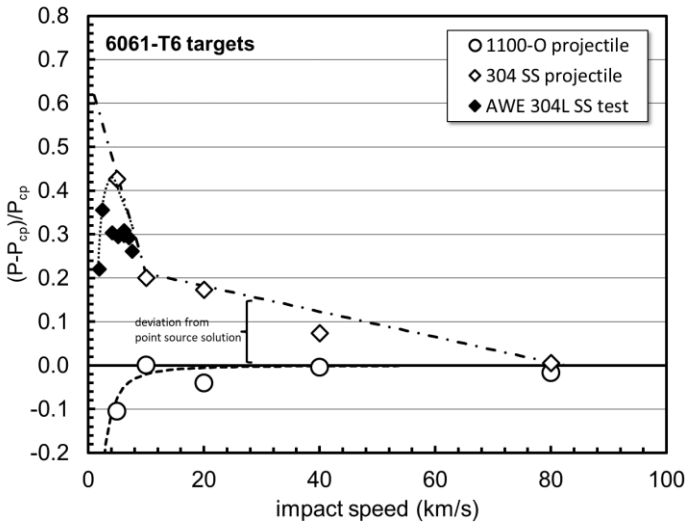

Fig. 2. Crater depth expressed as a difference from the coupling-parameter relation crater depth.

The broken curve is an empirical fit to the CTH calculations of steel spheres striking 6061-T6 targets. The equation describing the fit is

$$\frac{P-P_{cp}}{P_{cp}} = \begin{cases} 0.24 - 0.002917\, U\cos\beta & U\cos\beta > 10\ \text{km/s} \\ 0.664 - 0.04554\, U\cos\beta & U\cos\beta \le 10\ \text{km/s} \end{cases} \tag{7}$$

The normalized difference is set to zero whenever the result is less than zero.

The dashed curve is an empirical fit to the CTH calculations of aluminum spheres striking 6061-T6 targets. The equation describing the fit is

$$\frac{P-P_{cp}}{P_{cp}} = \exp(1/(-0.62\{U\cos\beta\}^{1.9})) - 1 \tag{8}$$

This completes the derivation of f in Eq. 2.

The filled symbols in Fig. 2 are Harrison et al [12] test data. The present authors added the dotted line to indicate the data trend, i.e., the normalized difference rises from 5 km/s to 3-km/s, rolls over at 3-km/s and then approaches zero as the impact speed approaches zero. The authors do not model this feature because the smallest meteoroid impact speed with respect to spacecraft in Earth orbit is near 5 km/s, hence this feature is outside of the range of application.

Figure 3 shows the results of the CTH crater diameter calculations expressed as a ratio of crater depth to crater diameter. The square on point symbols plot the CTH crater diameters for 304 stainless steel spheres striking 6061-T6 targets. Again, these calculations show that the steel projectiles do not result in the large speed power-law scaling except for speeds larger than those characteristic of meteoroids striking spacecraft in Earth orbit. The circle symbols plot the CTH crater diameters for 1100-0 commercially pure aluminum spheres striking 6061-T6 targets. Again, the aluminum projectile crater depths approach the large speed power-law scaling limit for 5-km/s impact speeds and larger.

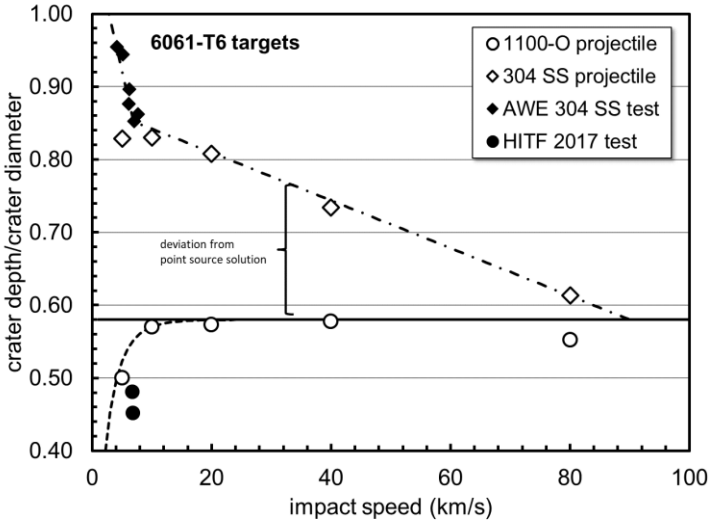

Fig. 3. Crater depth to diameter ratio as a function of impact speed.

The broken curve is an empirical fit to the CTH calculations of steel spheres striking 6061-T6 targets. The equation describing the fit is

$$\frac{P}{D} = \begin{cases} 0.875 - 0.003278\, U\cos\beta & U\cos\beta > 7\ \mathrm{km/s} \\ 1.10 - 0.03571\, U\cos\beta & U\cos\beta \le 7\ \mathrm{km/s} \end{cases} \tag{9}$$

The ratio is set to 0.58 whenever the result is less than 0.58.

The dashed curve is an empirical fit to the CTH calculations of aluminum spheres striking 6061-T6 targets. The equation describing the fit is

$$\frac{P}{D} = 0.58 \times \{1 - \exp(-0.61853\{U\cos\beta\}^{0.82})\} \tag{10}$$

This completes the derivation of g in Eq. 3.

The filled square on point symbols in Fig. 3 are plots of Harrison et al [13] test data. The filled circle symbols plot Christiansen et al data. [13] The agreement of test and calculation is fair.

The authors will take the expediency of linearly interpolating between the steel and the aluminum projectile curves for meteoroid densities between steel and aluminum. They further more assume that all meteoroids densities less than aluminum produce craters identical to those produced by aluminum projectiles when impacted by meteoroids with the same diameter as an aluminum projectile.

3 COMPARISON WITH LDEF

Figure 4 compares the crater counts from Humes [14] LDEF S0001 experiment (open circles and squares) with the results from Bumper [15] calculations using the MEM 3 meteoroid environment [16] and the Cour-Palais [1] crater dimension scaling relation (broken line) and the author's scaling relations (solid line). The error bars on the measurements are the standard deviations computed assuming the measured values are the means in a Poisson distribution.

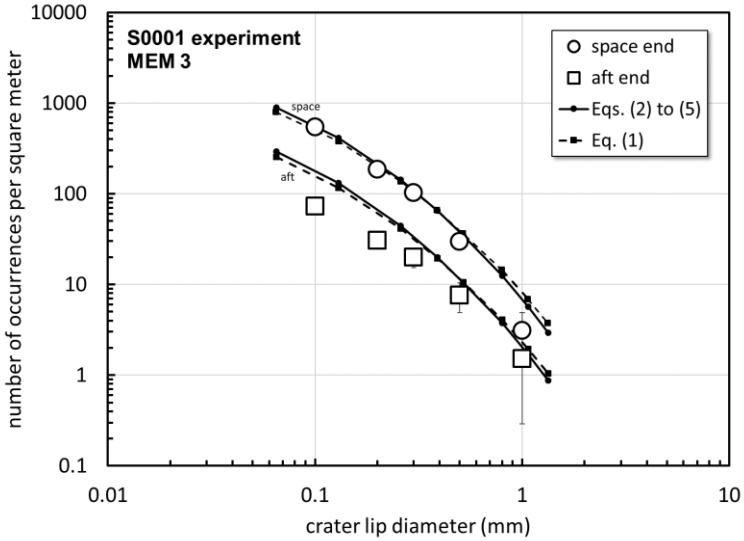

Fig. 4. LDEF experiment S0001 crater counts per unit area.

Following Moorhead et al [16], the authors assumed that meteoroids made all craters on the LDEF space end and that meteoroids made 90% of the craters on the aft side. Humes [14] measured the crater lip diameter and not the crater diameter nor the crater depth. Humes suggested that the crater diameter was 75% of the crater lip diameter for 1-mm crater lip diameters and that the crater diameter was 77% of the crater diameter for 500 μm crater lip diameters. The authors used 77% for all crater lip diameters less than or equal to 500 μm and 75% for all crater lip diameters greater than 500 μm.

On average, the space end predictions are within 32%, with the largest difference a factor of 2.2. The aft end predictions are within 80% on average, with the largest difference a factor of 2.4.

4 DISCUSSION

The Cour-Palais [1] cratering relation and the one developed for this paper fit the LDEF 20001 experiment results with equal accuracy using the MEM 3 environment. The authors repeated the analysis with the MEM release 2 environment that uses one meteoroid density (1 g/cm^3). The cratering relation developed for this paper resulted in 21% to 37% more craters than the Cour-Palais cratering relation and about 25% fewer craters than predicted with the MEM 3 environment. Again, the differences are smaller than the up to a factor of two differences from the observations. Thus, either BLE appears suitable to estimating crater counts.

The effect from using a fit based on calculations with projectiles with densities 2.7 g/cm^3 and larger was tested. The authors had performed calculations with nylon (1.14 g/cm^3) projectiles striking 1100-O targets. The authors strength-scaled the 1100-O results and added them to the fit, linearly interpolating between the aluminum and nylon projectile fits for meteoroid densities between 2.7 g/cm^3 and 1.14 g/cm^3. The authors set meteoroid mass densities less than 1.14 g/cm^3 equal to 1.14 g/cm^3. These changes to the BLE resulted in a couple of percent changes to the crater count results plotted in Fig.4. MEM 3 predicts that meteoroids with mass density larger than 2 g/cm^3 produce 70% of the craters on the space and aft ends of LDEF. Thus adding effects from meteoroid mass densities less than 2.8 g/cm^3 has little effect.

The authors attempted to evaluate the effect from ignoring plastic strain rate. However, they were unable to find a constitutive equation that was stable when evaluating the large plastic strain rates that occur during microcratering. With fixed everything else the plastic strain increases with inverse proportion to the projectile diameter. Thus, decreasing the projectile diameter from 1-mm to 1-μm will increase the plastic strain rate by a factor of 1,000. Now the strain rate of metals for cratering can be described by two power-law relations between yield stress and plastic strain rate: for plastic strain rates less than 10^3 s^{-1} the plastic strain rate exponent is small (0.01 to 0.1) and for plastic strain rates greater than 10^3 s^{-1} the plastic strain rate exponent is large (0.25 to 1). Thus, there is a sharp change in projectile size dependence from negligible for projectiles greater than 100 μm in diameter to significant for

projectiles less than 10 μm in diameter. Therefore, the authors caution the user to apply this cratering relation to projectiles larger than 100 μm.

5 CONCLUSIONS

The authors developed crater dimension scaling relationships that

1. Have the correct asymptotic limit as the impact speed increases
2. Remove the early time variables from the asymptotic limit of the crater dimension scaling.

The authors showed that the calculated number of craters in the LDEF S0001 experiment is insensitive to the crater diameter scaling relation.

6 ACKNOLEDGEMENT

The author thanks Althea Moorhead of the NASA Meteoroid Environment Office for providing the LDEF MEM 3 igloo flux file used in the analyses.

7 REFERENCES

1. Cour-Palais, B.G. Hypervelocity Impact Investigations and Meteoroid Shielding Experience Related to Apollo and Skylab. In *Orbital Debris*, ed. by Kessler, D.J. and Su, S.Y., NASA Johnson Space Center; Houston, TX, NASA CP-2360, 1985, pp. 247-275.
2. Cour-Palais, B.G. Empirical Hypervelocity Equations Developed for Apollo. In *Compilation of Papers Presented at OART Meteoroid Impact and Penetration Workshop*, 1968, pp. 566-601
3. Dienes, J. K., and J. M. Walsh, Theory of impact: Some general principals and the method of Eulerian codes, in *High-Velocity Impact Phenomena*, Ed by R. Kinslow, p. 46-104, Academic Press, Orlando, Fla, 1970.
4. Holsapple, K.A, and Schmidt, R.M. Point Source Solutions and Coupling Parameters in Cratering Mechanics. *J. Geophys. Res.*, Vol 92 No. B7, June 10, 1987. .p-6350-6376
5. Horz, F., Cintala, M.J., Bernhard, R.P, Cardena, F., Davidson, W.E., Haynes, G., See, T.H., and Winkler, J.L. Penetration Experiments in Aluminum 1100 Targets Using Soda-Lime Glass Projectiles. NASA TM 104812, NASA, Washington DC, June 1995.
6. Westine, P.S. and Mullin, S.A. Scale Modelling of Hypervelocity Impact. *Int. J. Impact Engng.* Vol 5, 1987, pp. 693-701.
7. Housen, K.R. and Holsapple, K.A. Ejecta from Impact Craters. *Icarus*, Vol 211, 2011 pp. 856-875
8. Schmitt, R.G., Brundage, A.L., Crawford, D.A., Harstad, E.N., Ruggirello, K., Schumacher, S.C. and Simmons, J.S. CTH User's Manual and Input Instructions. Ver 11.2. June 23, 2016. Sandia National Laboratories, Albuquerque, NM.
9. Kerley, G.I., Theoretical Equation of State for Aluminum, Int. J. Impact Engng. Vol. 5, 1987, pp. 441-449
10. Kerley, G.I., "Multiphase Equation of State for Iron," Sandia National Laboratories report SAND93-0227, 1993
11. Steinberg, D.J. Equation of State and Strength Properties of Selected Materials. UCRL-MA-106439 Change 1. Lawrence Livermore National Laboratory, Livermore CA. Feb 13, 1996.
12. Harrison, W., Loupias, C., Outrebon, P. and Turland, D. Experimental Data and Hydrocode Calculations for Hypervelocity Impacts of Stainless Steel into Aluminium in the 2-8 km/s Range. Int. J. Impact Engng. Vol 17, 1995, pp 363-374.
13. Christiansen, E.L., Cykowski, E. and Ortega, J. Highly Oblique Impacts into Thick and Thin Targets. Int. J. Impact Engng. Vol 14, 1993, pp 157-168.
14. Humes, D.H. "Large Craters on the Meteoroid and Space Debris Impact Experiment." in *LDEF – 69 Months in Space, First Post–Retrieval Symposium*, Part 1, ed. by A.S. Levine, NASA CP–3134 Part 1, National Aeronautics and Space Administration, Washington, DC, 1991, pp 399 – 418.

15. Bjorkman, M.D., Christiansen, E.L., and Lear, D.M., Bumper 3 Software User Manual. NASA Johnson Space Center, Houston, TX, NASA/TM-2014-218559. October 2014.

16. Moorhead, A.V., Kingery, A., Ehlert, S. NASA's Meteoroid Engineering Model (MEM) 3.0 and its Ability to Replicate Spacecraft Impact Rates. To be published in the Journal of Spacecraft and Rockets.